

Supporting Information:

**Pinacolone-alcohol gas-phase
solvation balances as experimental
dispersion benchmarks**

C. Zimmermann, T. L. Fischer, M. A. Suhm*

E-mail: msuhm@gwdg.de

Table S1: ORCA 4.2.1^{S1} and Turbomole^{S2,S3} keywords used for the different electronic structure calculations, optimizations, transition state searches (TS) and relaxed scans (RS).

| Level of approximation | Employed keywords |
|---|---|
| B3LYP-D3(BJ,ABC)/def2-TZVP (ORCA) | B3LYP D3BJ def2-TZVP abc grid5 NoFinalGrid UseSym VERYTIGHTSCF TIGHTOPT FREQ |
| B3LYP-D3(BJ,ABC)/def2-QZVP (ORCA) | B3LYP D3BJ def2-QZVPP abc grid5 NoFinalGrid UseSym VERYTIGHTSCF TIGHTOPT FREQ |
| DLPNO-CCSD(T) (ORCA) | DLPNO-CCSD(T) TightPNO aug-cc-pVQZ aug-cc-pVQZ/C TightSCF LED |
| TPSS-D3(BJ,ABC)/def2-TZVP (ORCA) | TPSS D3BJ def2-TZVP abc grid5 NoFinalGrid UseSym VERYTIGHTSCF TIGHTOPT NumFreq |
| TPSS-D3(BJ,ABC)/def2-QZVP (ORCA) | TPSS D3BJ def2-QZVPP abc grid5 NoFinalGrid UseSym VERYTIGHTSCF TIGHTOPT NumFreq |
| B97-3c-D3(BJ,ABC)/def2-mTZVP (TURBOMOLE) ^{TS} | b973c def2-mTZVP grid m5 disp3 bj abc ri itrvec 1 |
| B3LYP-D3(BJ,ABC)/def2-TZVP (ORCA) ^{TS} | B3LYP D3BJ def2-TZVP abc grid5 NoFinalGrid UseSym OptTS VERYTIGHTSCF TIGHTOPT FREQ |
| B3LYP-D3(BJ,ABC)/def2-TZVP (TURBOMOLE) ^{RS} | b3-lyp def2-mTZVP grid m5 disp3 bj abc ri |

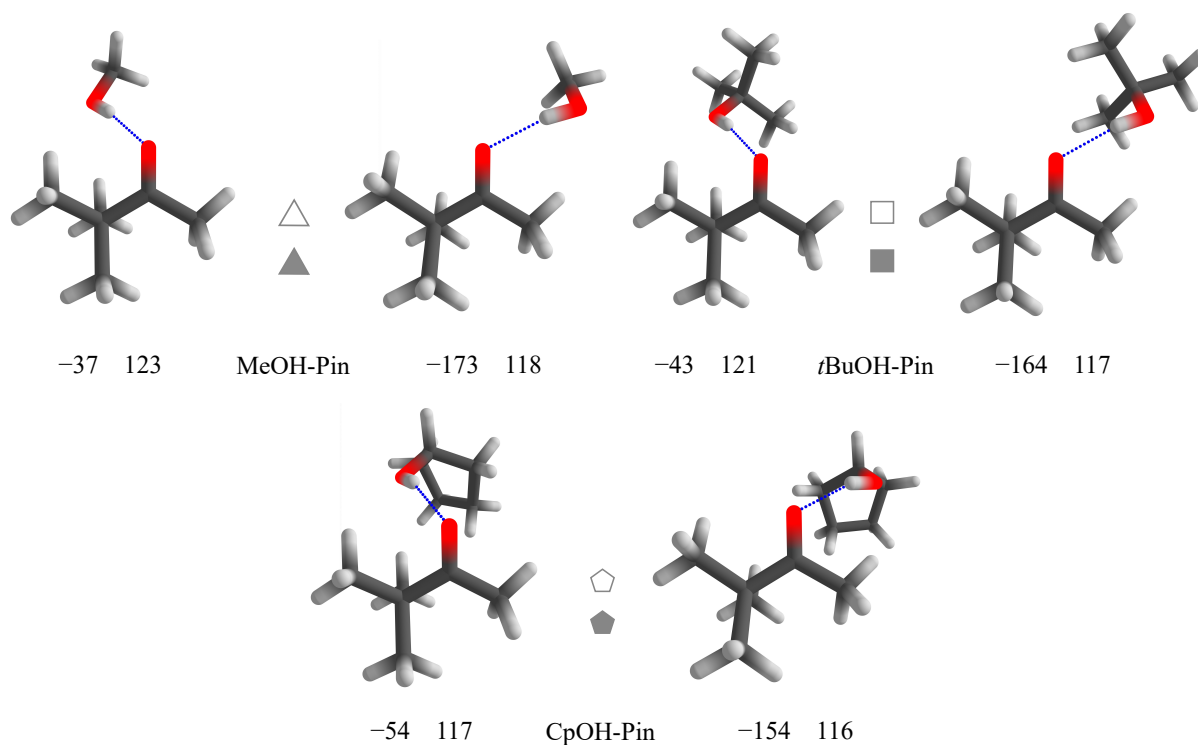


Fig. S1: Structures of the most stable alcohol-pinacolone dimers at B3LYP-D3(BJ,abc)/def2-TZVP level with the symbols used for them in the main text. Also given is the torsional angle τ of the hydrogen-bonded H relative to the *tert*-butyl group around the C=O group (C-C=O \cdots H, left value; the uniformly negative sign indicates that the solvating alcohol is pointing away from the reader) and the hydrogen bond angle α (C=O \cdots H, right value), both in $^\circ$.

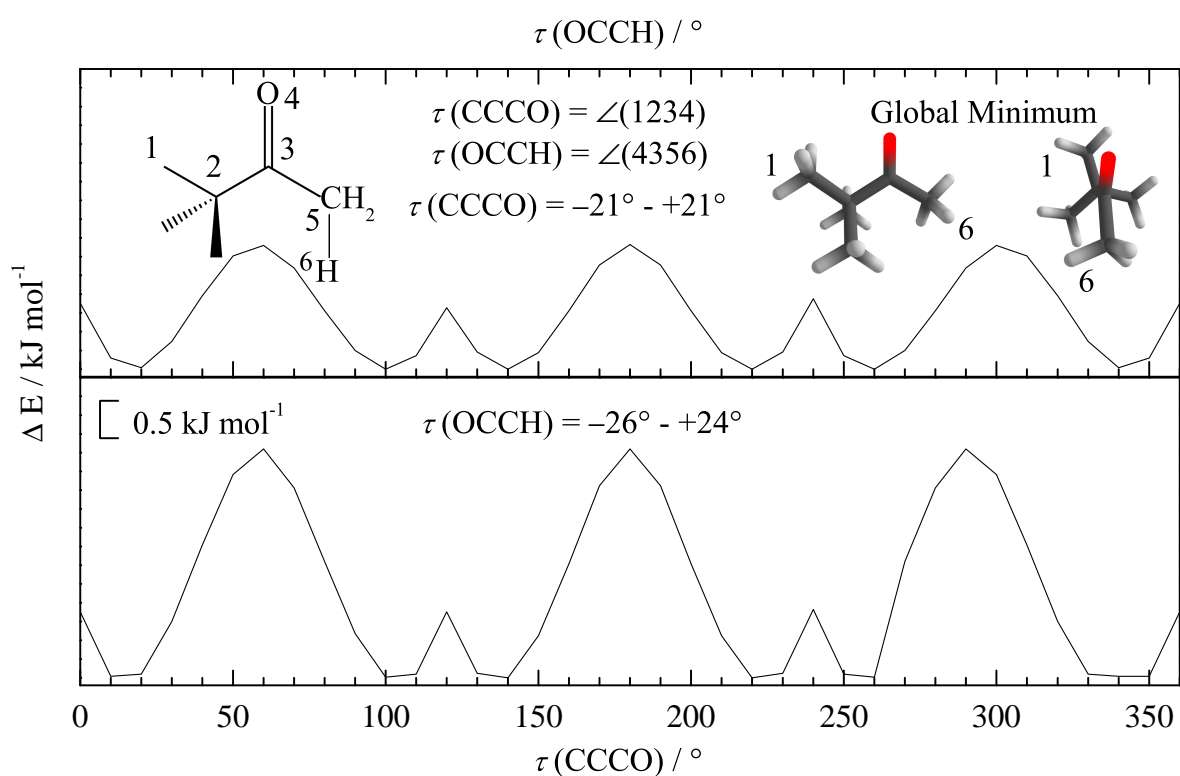


Fig. S2: Relaxed B3LYP-D3(BJ,ABC)/def2-TZVP scans along the OCCH (upper panel) and CCCO (lower panel) torsional angle for pinacolone monomer (with symmetry-breaking minima near 20° , 100° , 140° , 220° , 260°). In a jet expansion, barriers below 4 kJ mol^{-1} can be largely overcome. This suggests that also in complexes with alcohols, the pinacolone isomerism can be relaxed efficiently and leads to no additional spectral complexity.

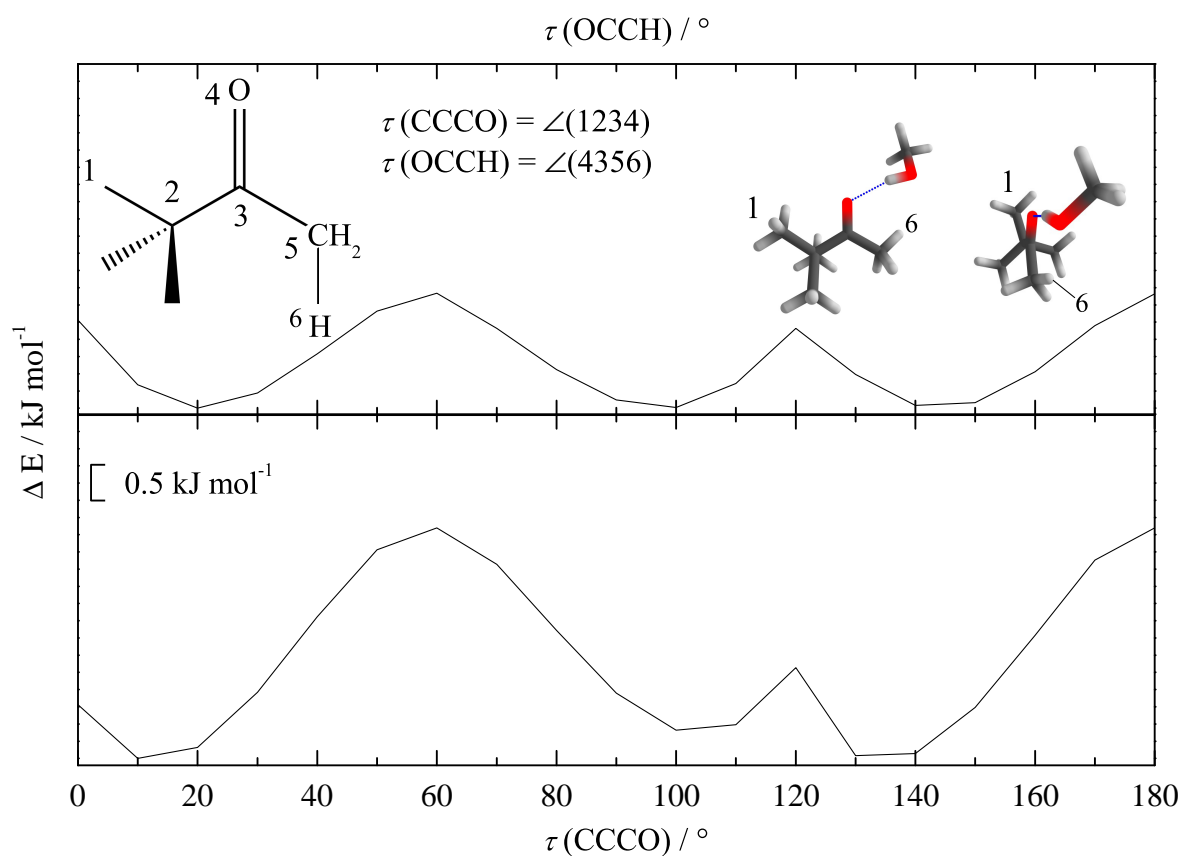


Fig. S3: Relaxed B3LYP-D3(BJ,ABC)/def2-TZVP scans along the OCCH (upper panel) and CCCO (lower panel) torsional angle for the Me-sided MeOH-pinacolone dimer structures. The persistently low barriers confirm that in complexes with alcohols, the pinacolone isomerism can be relaxed efficiently and likely leads to no additional spectral complexity.

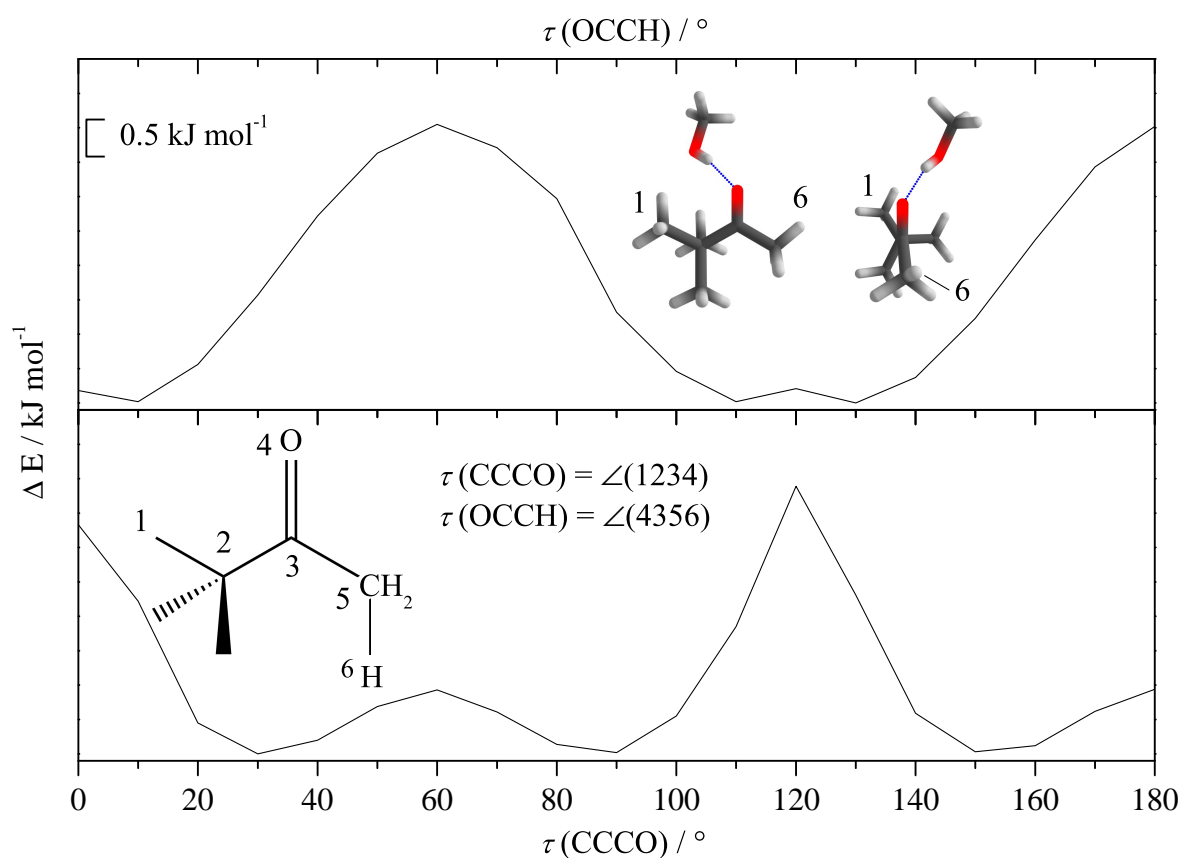


Fig. S4: Relaxed B3LYP-D3(BJ,ABC)/def2-TZVP scans along the OCCH (upper panel) and CCCO (lower panel) torsional angle for the *t*Bu-sided MeOH-pinacolone dimer structure, further confirming the insignificance of pinacolone isomerism for this study.

Table S2: Values for the hydrogen bond angle α between the ketone group and the hydrogen bonded H, and the associated H/*t*Bu torsional angle τ around the ketone group in $^\circ$. The negative sign for τ corresponds to Fig. S1, where the alcohol substituent is pointing away from the reader. With increasing alcohol size, the torsional angle deviates further from planarity. For comparison, the angles in the CpOH complex with acetone (Me docking only) are $\alpha=117^\circ$ and $\tau=-177^\circ$ at B3LYP/def2-TZVP level, so closer to the MeOH case.

| Donor | Method | basis set | <i>t</i> Bu | | Me | |
|---------------|--------------|-----------|-------------|----------|--------|----------|
| | | | τ | α | τ | α |
| MeOH | B3LYP-D3(BJ) | def2-TZVP | -37 | 123 | -173 | 118 |
| | B3LYP-D3(BJ) | def2-QZVP | -37 | 124 | -175 | 117 |
| | TPSS-D3(BJ) | def2-TZVP | -37 | 123 | -172 | 116 |
| | TPSS-D3(BJ) | def2-QZVP | -35 | 125 | -172 | 117 |
| <i>t</i> BuOH | B3LYP-D3(BJ) | def2-TZVP | -43 | 121 | -164 | 117 |
| | B3LYP-D3(BJ) | def2-QZVP | -44 | 120 | -163 | 117 |
| | TPSS-D3(BJ) | def2-TZVP | -45 | 120 | -163 | 116 |
| | TPSS-D3(BJ) | def2-QZVP | -45 | 120 | -163 | 116 |
| CpOH | B3LYP-D3(BJ) | def2-TZVP | -54 | 117 | -154 | 116 |
| | B3LYP-D3(BJ) | def2-QZVP | -55 | 116 | -153 | 116 |
| | TPSS-D3(BJ) | def2-TZVP | -51 | 117 | -154 | 115 |
| | TPSS-D3(BJ) | def2-QZVP | -55 | 117 | -153 | 115 |

Table S3: Methyl side docking preference in MeOH, *t*BuOH, CpOH-pinacolone complexes predicted by four DFT levels in kJ mol^{-1} relative to the *tert*-butyl side. ΔE^0 includes the harmonically approximated zero-point energy and ΔE^{el} excludes it. Negative values indicate a higher stability of the complex where the solvent docks on the methyl side of pinacolone. Zero-point energy corrections are typically small and do not change the isomer energy sequence. TPSS has a uniformly stronger methyl side docking preference than B3LYP.

| Donor | Method | def2-TZVP | | def2-QZVP | |
|---------------|--------------|---|-------------------------------------|---|-------------------------------------|
| | | $\Delta E_{\text{Me}-t\text{Bu}}^{\text{el}}$ | $\Delta E_{\text{Me}-t\text{Bu}}^0$ | $\Delta E_{\text{Me}-t\text{Bu}}^{\text{el}}$ | $\Delta E_{\text{Me}-t\text{Bu}}^0$ |
| MeOH | B3LYP-D3(BJ) | -1.39 | -1.40 | -1.58 | -1.59 |
| | TPSS-D3(BJ) | -2.27 | -2.04 | -2.22 | -2.16 |
| <i>t</i> BuOH | B3LYP-D3(BJ) | -0.66 | -0.62 | -0.80 | -0.75 |
| | TPSS-D3(BJ) | -1.50 | -1.32 | -1.66 | -1.51 |
| CpOH | B3LYP-D3(BJ) | -0.35 | -0.29 | -0.38 | -0.37 |
| | TPSS-D3(BJ) | -1.37 | -1.12 | -1.48 | -1.21 |

Table S4: Docking effect on the harmonic OH stretching wavenumbers ω and resulting wavenumber shifts $\Delta\omega$ for methyl (Me) and *tert*-butyl (*t*Bu) docking variants of alcohol-pinacolone complexes in cm^{-1} . Negative signs indicate a higher wavenumber for *tert*-butyl docking.

| Donor | Method | def2-TZVP | | | def2-QZVP | | |
|---------------|--------------|-----------|-------------|---------------------------------------|-----------|-------------|---------------------------------------|
| | | ω | | $\Delta\omega_{\text{Me}-t\text{Bu}}$ | ω | | $\Delta\omega_{\text{Me}-t\text{Bu}}$ |
| | | Me | <i>t</i> Bu | | Me | <i>t</i> Bu | |
| MeOH | B3LYP-D3(BJ) | 3616 | 3645 | -30 | 3627 | 3665 | -37 |
| | TPSS-D3(BJ) | 3472 | 3514 | -41 | 3482 | 3518 | -37 |
| <i>t</i> BuOH | B3LYP-D3(BJ) | 3617 | 3652 | -35 | 3635 | 3673 | -38 |
| | TPSS-D3(BJ) | 3469 | 3516 | -48 | 3478 | 3525 | -47 |
| CpOH | B3LYP-D3(BJ) | 3643 | 3695 | -51 | 3663 | 3714 | -51 |
| | TPSS-D3(BJ) | 3497 | 3548 | -50 | 3507 | 3570 | -63 |

Table S5: Methyl side coordination preference for different explored alcohol-pinacolone and acetylene-pinacolone complexes predicted at B3LYP-D3(BJ,abc)/def2-TZVP level relative to the *tert*-butyl side. ΔE^0 includes the harmonically approximated zero-point energy and ΔE^{el} excludes it. Zero-point energy corrections are typically small and do not change the energy sequence of the docking isomers. The preferred coordination is located on the methyl side of the pinacolone molecule for all presented systems, as shown by the uniformly negative sign. Also shown are harmonically predicted wavenumber differences $\Delta\omega_{\text{Me-}t\text{Bu}}$ between the docking sides, again uniformly negative. This shows that Me docking is always further downshifted in agreement with the higher stability. The shift is always predicted large enough to be experimentally resolved.

| Donor | Cas No. | $\Delta E_{\text{Me-}t\text{Bu}}^{\text{el}}$ | $\Delta E_{\text{Me-}t\text{Bu}}^0$ | $\Delta\omega_{\text{Me-}t\text{Bu}}$ |
|--|------------|---|-------------------------------------|---------------------------------------|
| Nonafluoro- <i>tert</i> -butyl alcohol | 2378-02-1 | -3.11 | -3.38 | -134 |
| 1,1,1,3,3,3-Hexafluoro-2-propanol (trans) | 920-66-1 | -3.38 | -3.41 | -111 |
| 1,1,1,3,3,3-Hexafluoro-2-propanol (gauche) | 920-66-1 | -1.86 | -1.87 | -112 |
| Cyclopropanol | 16545-68-9 | -2.09 | -1.78 | -14 |
| (-)-endo-Norborneol | 61277-90-5 | -2.00 | -1.75 | -68 |
| Prop-2-in-1-ol | 107-19-7 | -1.59 | -1.67 | -72 |
| 1-Methylcyclopentanol | 1462-03-9 | -2.23 | -1.63 | -60 |
| 2,2,2-Trifluoroethanol | 75-89-8 | -1.95 | -1.62 | -108 |
| Benzyl alcohol | 100-51-6 | -1.95 | -1.54 | -81 |
| 2-Methylcyclopentanol | 24070-77-7 | -1.93 | -1.53 | -21 |
| 2,5-Dimethylcyclopentanol (gauche) | 22417-55-6 | -1.58 | -1.47 | -35 |
| (S)-(-)-1-Phenylethanol | 1445-91-6 | -1.23 | -1.28 | -55 |
| Phenol | 108-95-2 | -0.98 | -1.23 | -62 |
| Cyclopropanemethanol | 2516-33-8 | -1.44 | -1.19 | -48 |
| 1-Adamantanol | 768-95-6 | -1.00 | -0.89 | -28 |
| Isopropyl alcohol (trans) | 67-63-0 | -0.87 | -0.81 | -38 |
| Isopropyl alcohol (gauche) | 67-63-0 | -0.56 | -0.50 | -38 |
| 2-Adamantanol | 700-57-2 | -0.20 | -0.49 | -23 |
| 2,5-Dimethylcyclopentanol (trans) | 22417-55-6 | -0.37 | -0.26 | -65 |

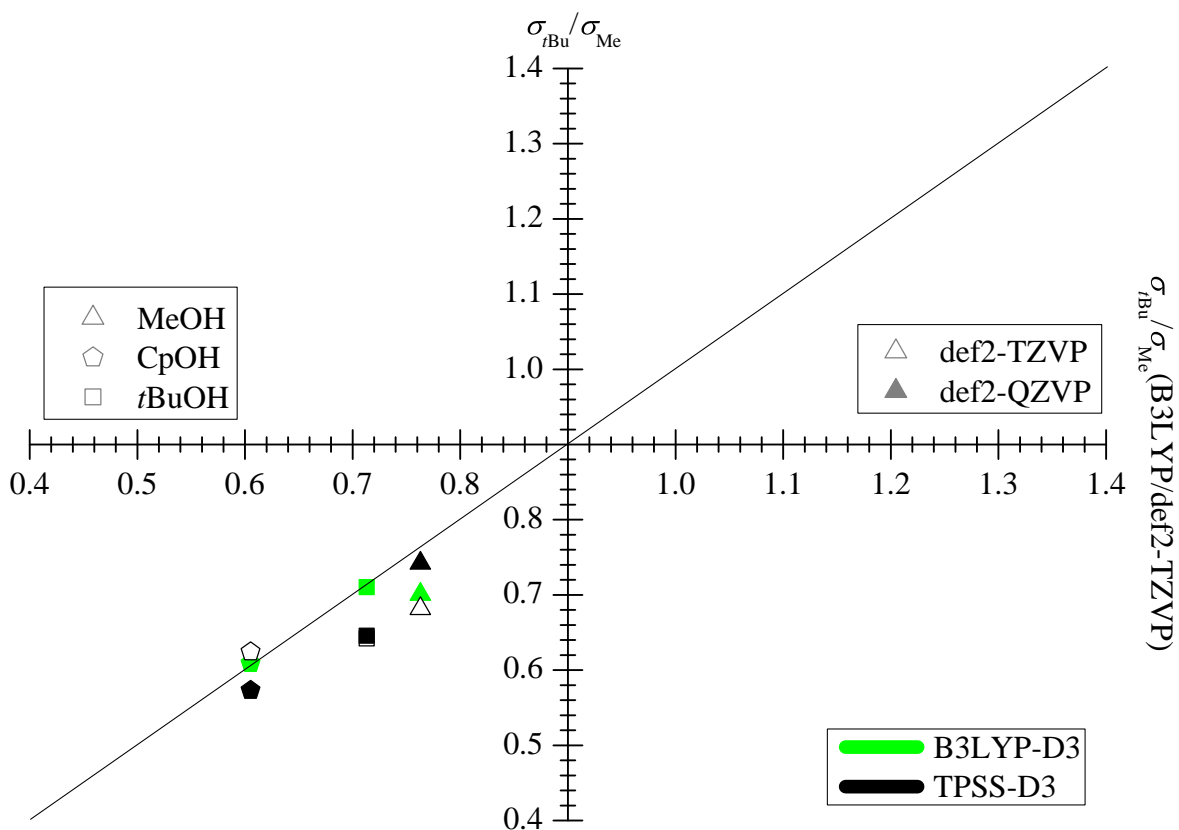


Fig. S5: B3LYP and TPSS infrared absorption cross section ratios $\sigma_{t\text{Bu}}/\sigma_{\text{Me}}$ with two different basis sets plotted against the B3LYP/def2-TZVP infrared absorption cross section ratios. The fairly good correlation along the bisector indicates that theoretical scatter in this quantity is small and the empty first quadrant shows that Me side docking always gives rise to stronger IR signals than *t*Bu side docking.

Table S6: Experimental OH stretching wavenumbers $\tilde{\nu}$ and resulting wavenumber shifts $\Delta\tilde{\nu}_{h-l}$ for high (h) and low (l) lying spectral signals for alcohol-pinacolone 1:1 complexes in cm^{-1} . These shifts are essential to judge the predictive performance of the different DFT levels.

| Donor | $\tilde{\nu}$ | | $\Delta\tilde{\nu}_{h-l}$ |
|---------------|---------------|------|---------------------------|
| | high | low | |
| MeOH | 3561 | 3522 | 38 |
| <i>t</i> BuOH | 3537 | 3505 | 32 |
| CpOH | 3567 | 3527 | 40 |

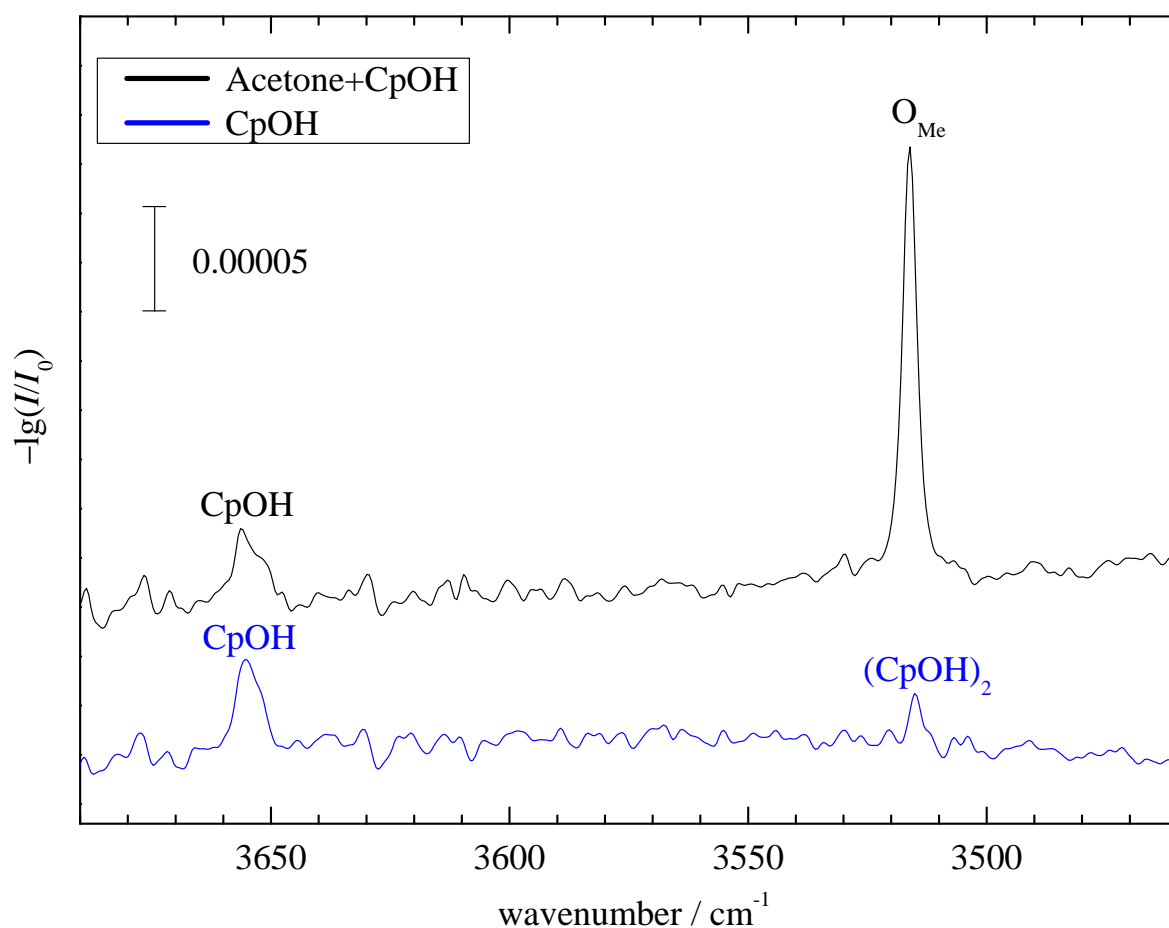


Fig. S6: OH stretching FTIR spectra of CpOH expansions in He with (black) and without acetone (blue) under otherwise identical experimental conditions. The signals of the homodimer (CpOH)₂ and of the 1:1 complex O_{Me} (no docking isomerism because of the symmetry of acetone) are seen to overlap almost perfectly. This overlap is removed for pinacolone, likely because the interaction of the Cp ring with the *t*Bu group on the other side of the ketone group distorts the hydrogen bond.

Table S7: Experimental range for the integrated intensity ratios $I_{\text{Me}}/I_{t\text{Bu}}$, with absorption cross-sections from theory (two different DFT functionals and basis sets), derived docking ratios $c_{\text{Me}}/c_{t\text{Bu}}$ and resulting experimental fractions $x_{t\text{Bu}}$ for *t*Bu docking. The minimal and maximal values for $I_{\text{Me}}/I_{t\text{Bu}}$ were received using an automated statistical evaluation^{S4} and were used to determine the span of possible $c_{\text{Me}}/c_{t\text{Bu}}$ and $x_{t\text{Bu}}$ values consistent with the spectra, assuming exact theoretical cross section ratios.

| Method | Donor | $\frac{I_{\text{Me}}}{I_{t\text{Bu}}}$ | $\frac{c_{\text{Me}}}{c_{t\text{Bu}}}$ | $x_{t\text{Bu}}$ |
|------------------------|---------------|--|--|------------------|
| B3LYP-D3(BJ)/def2-TZVP | MeOH | 5.91-11.82 | 4.51-9.02 | 0.10-0.18 |
| | <i>t</i> BuOH | 2.38-4.16 | 1.70-2.96 | 0.25-0.37 |
| | CpOH | 5.54-7.30 | 3.36-4.42 | 0.18-0.23 |
| B3LYP-D3(BJ)/def2-QZVP | MeOH | 5.91-11.82 | 4.14-8.28 | 0.11-0.19 |
| | <i>t</i> BuOH | 2.38-4.16 | 1.69-2.95 | 0.25-0.37 |
| | CpOH | 5.54-7.30 | 3.38-4.44 | 0.18-0.23 |
| TPSS-D3(BJ)/def2-TZVP | MeOH | 5.91-11.82 | 4.03-8.06 | 0.11-0.20 |
| | <i>t</i> BuOH | 2.38-4.16 | 1.53-2.67 | 0.27-0.40 |
| | CpOH | 5.54-7.30 | 3.46-4.56 | 0.18-0.22 |
| TPSS-D3(BJ)/def2-QZVP | MeOH | 5.91-11.82 | 4.39-8.77 | 0.10-0.19 |
| | <i>t</i> BuOH | 2.38-4.16 | 1.54-2.68 | 0.27-0.39 |
| | CpOH | 5.54-7.30 | 3.18-4.18 | 0.19-0.24 |

Table S8: Experimental range for the integrated intensity ratios $I_{t\text{Bu}}/I_{\text{Me}}$, with absorption cross-sections from theory (two different DFT functionals and basis sets), derived docking ratios $c_{t\text{Bu}}/c_{\text{Me}}$ and resulting experimental fractions x_{Me} for methyl docking. The minimal and maximal values for $I_{t\text{Bu}}/I_{\text{Me}}$ were obtained using an automated statistical evaluation^{S4} and were used to determine the span of possible $c_{t\text{Bu}}/c_{\text{Me}}$ and x_{Me} values consistent with the spectra. Differences to the inverse evaluation in Tab. S7 are small.

| Method | Donor | $\frac{I_{t\text{Bu}}}{I_{\text{Me}}}$ | $\frac{c_{t\text{Bu}}}{c_{\text{Me}}}$ | x_{Me} |
|------------------------|---------------|--|--|-----------------|
| B3LYP-D3(BJ)/def2-TZVP | MeOH | 0.08-0.17 | 0.11-0.22 | 0.82-0.90 |
| | <i>t</i> BuOH | 0.24-0.42 | 0.34-0.59 | 0.63-0.75 |
| | CpOH | 0.14-0.18 | 0.23-0.29 | 0.77-0.81 |
| B3LYP-D3(BJ)/def2-QZVP | MeOH | 0.08-0.17 | 0.12-0.24 | 0.81-0.89 |
| | <i>t</i> BuOH | 0.24-0.42 | 0.34-0.59 | 0.63-0.75 |
| | CpOH | 0.14-0.18 | 0.23-0.29 | 0.78-0.81 |
| TPSS-D3(BJ)/def2-TZVP | MeOH | 0.08-0.17 | 0.12-0.25 | 0.80-0.89 |
| | <i>t</i> BuOH | 0.24-0.42 | 0.37-0.65 | 0.61-0.73 |
| | CpOH | 0.14-0.18 | 0.23-0.28 | 0.78-0.82 |
| TPSS-D3(BJ)/def2-QZVP | MeOH | 0.08-0.17 | 0.11-0.23 | 0.81-0.90 |
| | <i>t</i> BuOH | 0.24-0.42 | 0.37-0.65 | 0.61-0.73 |
| | CpOH | 0.14-0.18 | 0.25-0.31 | 0.76-0.80 |

Table S9: Electronic dissociation energies of alcohol-pinacolone complexes for two different DFT functionals and basis sets in kJ mol^{-1} . Alcohol and docking variations are of comparable magnitude and the difference between the two docking options never exceeds 8%.

| Donor | Method | Me | <i>t</i> Bu |
|---------------|------------------------|------|-------------|
| MeOH | B3LYP-D3(BJ)/def2-TZVP | 33.4 | 32.0 |
| | B3LYP-D3(BJ)/def2-QZVP | 30.9 | 29.3 |
| | TPSS-D3(BJ)/def2-TZVP | 32.4 | 30.2 |
| | TPSS-D3(BJ)/def2-QZVP | 30.1 | 27.9 |
| <i>t</i> BuOH | B3LYP-D3(BJ)/def2-TZVP | 34.1 | 33.5 |
| | B3LYP-D3(BJ)/def2-QZVP | 31.8 | 31.0 |
| | TPSS-D3(BJ)/def2-TZVP | 32.9 | 31.4 |
| | TPSS-D3(BJ)/def2-QZVP | 30.7 | 29.1 |
| CpOH | B3LYP-D3(BJ)/def2-TZVP | 35.9 | 35.5 |
| | B3LYP-D3(BJ)/def2-QZVP | 33.6 | 33.2 |
| | TPSS-D3(BJ)/def2-TZVP | 33.8 | 32.4 |
| | TPSS-D3(BJ)/def2-QZVP | 31.7 | 30.2 |

Table S10: Effective conformational freezing temperatures T_c for alcohol-pinacolone systems, calculated with ZPVE corrected DFT energy differences (in parentheses based on DLPNO-CCSD(T) electronic energies from Tab. S12 instead of DFT electronic energies) and the band integral ratios obtained from experiment. Error bars were obtained from upper and lower band integral ratio bounds and chosen symmetrically. For the barriers expected in these systems, plausible T_c values are $\leq 150 \text{ kJ mol}^{-1}$.^{S5} and positive, but significantly higher than the rotational temperature of about 10 kJ mol^{-1} . A higher T_c indicates an overestimated energy gap (or an unexpectedly high barrier) and a very low T_c indicates an underestimated energy gap. B3LYP is thus seen to favour *t*Bu docking too much for CpOH and TPSS to disfavour *t*Bu somewhat for *t*BuOH. The CCSD(T) correction (in parentheses) switches the docking sequence for CpOH and lowers all *t*BuOH values too much, leaving only MeOH predictions in a plausible range.

| Donor | Method | def2-TZVP | def2-QZVP |
|---------------|--------------|---------------|---------------|
| | | T_c | T_c |
| | B3LYP-D3(BJ) | 94 ± 18 | 112 ± 22 |
| | | (44 ± 8) | (84 ± 16) |
| MeOH | TPSS-D3(BJ) | 147 ± 29 | 147 ± 28 |
| | | (55 ± 11) | (54 ± 10) |
| | B3LYP-D3(BJ) | 105 ± 36 | 128 ± 44 |
| | | (29 ± 10) | (19 ± 6) |
| <i>t</i> BuOH | TPSS-D3(BJ) | 268 ± 106 | 303 ± 118 |
| | | (4 ± 2) | (8 ± 3) |
| | B3LYP-D3(BJ) | 26 ± 3 | 33 ± 3 |
| | | (-29 ± 3) | (-20 ± 2) |
| CpOH | TPSS-D3(BJ) | 99 ± 10 | 113 ± 12 |
| | | (-20 ± 2) | (-26 ± 3) |

Table S11: LED analysis for the methyl and *tert*-butyl bound B3LYP and TPSS minimum structures at DLPNO-CCSD(T) level (single point computations) in kJ mol⁻¹. The interfragment dispersion contributions of strong and weak pairs (ORCA LED output) were combined to yield the total dispersion contribution to the intermolecular interaction. ΔD in the last column gives the difference in dispersion contribution between both docking sides. Its consistently positive value shows that the *tert*-butyl docking structure is offering more dispersion attraction than the corresponding methyl docking structure. CpOH profits most from this attraction, at least at B3LYP level.

| pre-optimization | | With D | Without D | |
|------------------------|---------------|---|---|------------|
| level | | $\Delta E_{\text{Me}-t\text{Bu}}^{\text{el}}$ | $\Delta E_{\text{Me}-t\text{Bu}}^{\text{el}}$ | ΔD |
| B3LYP-D3(BJ)/def2-TZVP | MeOH | -0.65 | -3.09 | +2.44 |
| | <i>t</i> BuOH | -0.21 | -2.39 | +2.19 |
| | CpOH | +0.26 | -2.88 | +3.14 |
| B3LYP-D3(BJ)/def2-QZVP | MeOH | -1.17 | -3.50 | +2.32 |
| | <i>t</i> BuOH | -0.16 | -2.53 | +2.37 |
| | CpOH | +0.21 | -2.91 | +3.13 |
| TPSS-D3(BJ)/def2-TZVP | MeOH | -0.99 | -3.12 | +2.12 |
| | <i>t</i> BuOH | -0.20 | -2.28 | +2.08 |
| | CpOH | -0.02 | -2.30 | +2.28 |
| TPSS-D3(BJ)/def2-QZVP | MeOH | -0.85 | -2.37 | +1.52 |
| | <i>t</i> BuOH | -0.19 | -2.42 | +2.23 |
| | CpOH | 0.00 | -2.33 | +2.33 |

Table S12: Energy advantage of methyl relative to *t*-butyl coordination of pinacolone by three alcohols at DFT and DLPNO-CCSD(T) corrected level in kJ mol⁻¹. ΔE^0 includes and ΔE^{el} excludes the harmonic DFT ZPVE. Higher stability for the *t*-butyl coordination (contradicting experiment) is indicated by a positive energy difference. The CCSD(T) correction leads to a systematic shift towards *t*-butyl docking, in particular for TPSS structures.

| Donor | Method | $\Delta E_{\text{Me}-t\text{Bu}}^{\text{el}}$ | $\Delta E_{\text{Me}-t\text{Bu}}^0$ |
|---------------|---------------------------------------|---|-------------------------------------|
| MeOH | B3LYP-D3(BJ)/def2-TZVP | -1.39 | -1.40 |
| | DLPNO-CCSD(T)//B3LYP-D3(BJ)/def2-TZVP | -0.65 | -0.66 |
| | B3LYP-D3(BJ)/def2-QZVP | -1.58 | -1.59 |
| | DLPNO-CCSD(T)//B3LYP-D3(BJ)/def2-QZVP | -1.17 | -1.19 |
| | TPSS-D3(BJ)/def2-TZVP | -2.27 | -2.04 |
| | DLPNO-CCSD(T)//TPSS-D3(BJ)/def2-TZVP | -0.99 | -0.76 |
| | TPSS-D3(BJ)/def2-QZVP | -2.22 | -2.16 |
| | DLPNO-CCSD(T)//TPSS-D3(BJ)/def2-QZVP | -0.85 | -0.78 |
| <i>t</i> BuOH | B3LYP-D3(BJ)/def2-TZVP | -0.66 | -0.62 |
| | DLPNO-CCSD(T)//B3LYP-D3(BJ)/def2-TZVP | -0.21 | -0.17 |
| | B3LYP-D3(BJ)/def2-QZVP | -0.80 | -0.75 |
| | DLPNO-CCSD(T)//B3LYP-D3(BJ)/def2-QZVP | -0.16 | -0.11 |
| | TPSS-D3(BJ)/def2-TZVP | -1.50 | -1.32 |
| | DLPNO-CCSD(T)//TPSS-D3(BJ)/def2-TZVP | -0.20 | -0.02 |
| | TPSS-D3(BJ)/def2-QZVP | -1.66 | -1.51 |
| | DLPNO-CCSD(T)//TPSS-D3(BJ)/def2-QZVP | -0.19 | -0.04 |
| CpOH | B3LYP-D3(BJ)/def2-TZVP | -0.35 | -0.29 |
| | DLPNO-CCSD(T)//B3LYP-D3(BJ)/def2-TZVP | +0.26 | +0.32 |
| | B3LYP-D3(BJ)/def2-QZVP | -0.38 | -0.37 |
| | DLPNO-CCSD(T)//B3LYP-D3(BJ)/def2-QZVP | +0.21 | +0.23 |
| | TPSS-D3(BJ)/def2-TZVP | -1.37 | -1.12 |
| | DLPNO-CCSD(T)//TPSS-D3(BJ)/def2-TZVP | -0.02 | +0.23 |
| | TPSS-D3(BJ)/def2-QZVP | -1.48 | -1.21 |
| | DLPNO-CCSD(T)//TPSS-D3(BJ)/def2-QZVP | 0.00 | +0.28 |

Table S13: D3 contribution analysis in kJ mol^{-1} to the energy advantage of the methyl side at the D3-inclusive optimized structures after zero point energy correction for the B3LYP and TPSS functionals. ΔD3 in the last column gives the dispersion correction advantage for *tert*-butyl docking. A positive value means that the *tert*-butyl docking structure offers more D3 attraction than the corresponding methyl docking structure. The effects are quite similar to those of the LED analysis in Tab. S11.

| | Donor | With D3 | | Without D3 | | ΔD3 |
|--------------|---------------|---|-------------------------------------|---|-------------------------------------|-------------------|
| | | $\Delta E_{\text{Me}-t\text{Bu}}^{\text{el}}$ | $\Delta E_{\text{Me}-t\text{Bu}}^0$ | $\Delta E_{\text{Me}-t\text{Bu}}^{\text{el}}$ | $\Delta E_{\text{Me}-t\text{Bu}}^0$ | |
| B3LYP-D3(BJ) | MeOH | -1.39 | -1.40 | -3.44 | -3.44 | +2.05 |
| | <i>t</i> BuOH | -0.66 | -0.62 | -2.79 | -2.76 | +2.14 |
| | /def2-TZVP | CpOH | -0.35 | -0.29 | -3.13 | -3.07 |
| B3LYP-D3(BJ) | MeOH | -1.58 | -1.59 | -3.94 | -3.95 | +2.37 |
| | <i>t</i> BuOH | -0.80 | -0.75 | -2.43 | -2.38 | +1.63 |
| | /def2-QZVP | CpOH | -0.38 | -0.37 | -3.17 | -3.15 |
| TPSS-D3(BJ) | MeOH | -2.27 | -2.04 | -4.24 | -4.02 | +1.98 |
| | <i>t</i> BuOH | -1.50 | -1.32 | -3.12 | -2.94 | +1.62 |
| | /def2-TZVP | CpOH | -1.37 | -1.12 | -3.07 | -2.82 |
| TPSS-D3(BJ) | MeOH | -2.22 | -2.16 | -3.75 | -3.69 | +1.53 |
| | <i>t</i> BuOH | -1.66 | -1.51 | -3.27 | -3.13 | +1.61 |
| | /def2-QZVP | CpOH | -1.48 | -1.21 | -3.31 | -3.03 |

Table S14: Exploration of alternative CpOH docking structures (Me1, *t*Bu1). Docking energy advantages in kJ mol^{-1} without (ΔE^{el}) and with (ΔE^0) zero point energy correction and corresponding wavenumber shifts $\Delta\omega$ in cm^{-1} predicted by four DFT levels. Positive energy values indicate a higher stability of the second docking variant listed under Comparison. Me1-*t*Bu1 appears to fit experiment (Tab. S6) better than Me-*t*Bu in relative energy and shifts. However, DLPNO-CCSD(T) level calculations (see Tab. S15) discourage this alternative.

| Comparison | Method | def2-TZVP | | | def2-QZVP | | |
|---------------------------|--------------|------------------------|--------------|----------------|------------------------|--------------|----------------|
| | | ΔE^{el} | ΔE^0 | $\Delta\omega$ | ΔE^{el} | ΔE^0 | $\Delta\omega$ |
| Me- <i>t</i> Bu | B3LYP-D3(BJ) | -0.35 | -0.29 | -51 | -0.38 | -0.37 | -51 |
| | TPSS-D3(BJ) | -1.37 | -1.12 | -50 | -1.48 | -1.21 | -63 |
| Me1- <i>t</i> Bu1 | B3LYP-D3(BJ) | -1.03 | -0.98 | -38 | -0.94 | -0.93 | -40 |
| | TPSS-D3(BJ) | -1.50 | -1.23 | -43 | -1.36 | -1.36 | -36 |
| Me-Me1 | B3LYP-D3(BJ) | -1.38 | -1.07 | +23 | -1.28 | -1.02 | +25 |
| | TPSS-D3(BJ) | -1.18 | -1.00 | +23 | -1.02 | -0.89 | +22 |
| <i>t</i> Bu- <i>t</i> Bu1 | B3LYP-D3(BJ) | -2.05 | -1.76 | +35 | -1.84 | -1.59 | +36 |
| | TPSS-D3(BJ) | -1.31 | -1.10 | +31 | -0.90 | -1.05 | +48 |
| Me1- <i>t</i> Bu | B3LYP-D3(BJ) | +1.02 | +0.77 | -75 | +0.90 | +0.65 | -75 |
| | TPSS-D3(BJ) | -0.19 | -0.12 | -74 | -0.46 | -0.32 | -85 |
| Me- <i>t</i> Bu1 | B3LYP-D3(BJ) | -2.40 | -2.05 | -15 | -2.22 | -1.95 | -15 |
| | TPSS-D3(BJ) | -2.68 | -2.23 | -19 | -2.38 | -2.25 | -15 |

Table S15: Ruling out alternative CpOH docking structures (Me1, *t*Bu1) explored in Tab. S14 based on DLPNO-CCSD(T) single point calculations at the structures obtained by different preoptimization (Preopt.) methods. The energy penalty of both alternatives (in kJ mol^{-1}) further increases. Also given is the difference in dispersion contribution ΔD between the docking sides as in Tab. S11. Positive values indicate more dispersion interaction in the second docking variant listed than in the first. Me1 and *t*Bu1 are thus less dispersively bound.

| Comparison | Preopt. | def2-TZVP | | def2-QZVP | |
|---------------------------|--------------|--------------------------|------------|--------------------------|------------|
| | | $\Delta E^{\text{el+D}}$ | ΔD | $\Delta E^{\text{el+D}}$ | ΔD |
| Me- <i>t</i> Bu | B3LYP-D3(BJ) | +0.26 | +3.14 | +0.21 | +3.13 |
| | TPSS-D3(BJ) | -0.02 | +2.28 | 0.00 | +2.33 |
| Me1- <i>t</i> Bu1 | B3LYP-D3(BJ) | -0.26 | +2.71 | -0.30 | +2.30 |
| | TPSS-D3(BJ) | -0.27 | +2.85 | -0.57 | +2.16 |
| Me-Me1 | B3LYP-D3(BJ) | -1.93 | -4.93 | -1.93 | -4.95 |
| | TPSS-D3(BJ) | -1.93 | -4.54 | -1.92 | -4.14 |
| <i>t</i> Bu- <i>t</i> Bu1 | B3LYP-D3(BJ) | -2.44 | -5.36 | -2.44 | -5.79 |
| | TPSS-D3(BJ) | -2.18 | -3.97 | -2.49 | -4.31 |
| Me1- <i>t</i> Bu | B3LYP-D3(BJ) | +2.20 | +8.06 | +2.15 | +8.08 |
| | TPSS-D3(BJ) | +1.92 | +6.82 | +1.92 | +6.47 |
| Me- <i>t</i> Bu1 | B3LYP-D3(BJ) | -2.20 | -2.22 | -2.23 | -2.66 |
| | TPSS-D3(BJ) | -2.20 | -1.69 | -2.49 | -1.98 |

References

- (S1) Neese, F. Software update: the ORCA program system, version 4.0. *WIREs Comput. Mol. Sci.* **2018**, *8*, e1327.
- (S2) TURBOMOLE V7.3 2018, a development of University of Karlsruhe and Forschungszentrum Karlsruhe GmbH, 1989-2007, TURBOMOLE GmbH, since 2007; available from <http://www.turbomole.com>.
- (S3) Furche, F.; Ahlrichs, R.; Hättig, C.; Klopper, W.; Sierka, M.; Weigend, F. Turbomole. *WIREs Comput. Mol. Sci.* **2014**, *4*, 91–100.
- (S4) Karir, G.; Lüttschwager, N. O. B.; Suhm, M. A. Phenylacetylene as a gas phase sliding balance for solvating alcohols. *Phys. Chem. Chem. Phys.* **2019**, *21*, 7831–7840.
- (S5) Poblitzki, A.; Gottschalk, H. C.; Suhm, M. A. Tipping the Scales: Spectroscopic Tools for Intermolecular Energy Balances. *The Journal of Physical Chemistry Letters* **2017**, *8*, 5656–5665.